Construction of multifunctional porcine acellular dermal matrix hydrogel blended with vancomycin for hemorrhage control, antibacterial action, and tissue repair in infected trauma wounds

D. Cai [a,1], S. Chen [a,1], B. Wu [a,1], J. Chen [b], D. Tao [c], Z. Li [c], Q. Dong [a], Y. Zou [a], Y. Chen [a,d], C. Bi [a,d], D. Zu [e,***], L. Lu [a,**], B. Fang [a,*]

[a] Department of Spine Surgery, The Central Hospital Affiliated to Shaoxing University, Shaoxing, China
[b] Bacterial Laboratory, The Central Hospital Affiliated to Shaoxing University, Shaoxing, China
[c] Pathology Department, The Central Hospital Affiliated to Shaoxing University, Shaoxing, China
[d] School of Medcine, Shaoxing University, Shaoxing, China
[e] Central Laboratory, The Central Hospital Affiliated to Shaoxing University, Shaoxing, China

ABSTRACT

Prevention of bacterial infection and reduction of hemorrhage, the primary challenges posed by trauma before hospitalization, are essential steps in prolonging the patient's life until they have been transported to a trauma center. Extracellular matrix (ECM) hydrogel is a promising biocompatible material for accelerating wound closure. However, due to the lack of antibacterial properties, this hydrogel is difficult to be applied to acute contaminated wounds. This study formulates an injectable dermal extracellular matrix hydrogel (porcine acellular dermal matrix (ADM)) as a scaffold for skin defect repair. The hydrogel combines vancomycin, an antimicrobial agent for inducing hemostasis, expediting antimicrobial activity, and promoting tissue repair. The hydrogel possesses a porous structure beneficial for the adsorption of vancomycin. The antimicrobial agent can be timely released from the hydrogel within an hour, which is less than the time taken by bacteria to infest an injury, with a cumulative release rate of approximately 80%, and thus enables a relatively fast bactericidal effect. The cytotoxicity investigation demonstrates the biocompatibility of the ADM hydrogel. Dynamic coagulation experiments reveal accelerated blood coagulation by the hydrogel. In vivo antibacterial and hemostatic experiments on a rat model indicate the healing of infected tissue and effective control of hemorrhaging by the hydrogel. Therefore, the vancomycin-loaded ADM hydrogel will be a viable biomaterial for controlling hemorrhage and preventing bacterial infections in trauma patients.

1. Introduction

Uncontrolled bleeding is the leading cause of death among trauma patients, with approximately 33%–56% of the deaths occurring during the phase before hospitalization [1]. Without appropriate intervention, trauma-related bleeding can induce a series of systemic reactions and acute coagulopathy in the wound, which may prove fatal to the patient [2,3]. Timely and effective emergency hemostasis even before hospitalization can provide valuable time for the subsequent treatment, thereby reducing the chances of disability or mortality. Currently, HemCon and QuikClot are widely used as hemostatic materials in fields such as defense where trauma injuries are common [4–6]. However, these materials do not have sufficient durability to prevent uncontrolled bleeding from blood vessels. In addition, they often bring inevitable side-effects such as high rebleeding rates (HemCon) [4] and tissue thermal damage (Quikclot) [5], which severely limit their further application. Moreover, wounds exposed to a polluted environment are prone to bacterial infection [7–9], which can hinder the healing process and cause life-threatening complications including sepsis, severe sepsis, and septic shock [10,11]. Nevertheless, bacterial infection receives relatively less

focus in the treatment stage prior to hospitalization than hemorrhage [11]. Thus, treatment before hospitalization faces the dual challenges of controlling bleeding and preventing microbial infection. Therefore, developing a novel biomaterial that can effectively control hemorrhage and rapidly prevent microbial growth in the emergency stage prior to hospitalization is important for trauma care.

Research on the development of antimicrobial and hemostatic materials is gaining prominence. For example, studies have demonstrated the use of silver (Ag) ions as a broad-spectrum antimicrobial agent [12–14] that can inhibit the growth of fungi, gram-positive bacteria, gram-negative bacteria, and viruses, and these have since become common in biomedical applications. Ong et al. [15] refined the chitosan dressing by combining a coagulant (polyphosphate) and Ag nanoparticles (NPs) to achieve hemostatic and antimicrobial effects. However, Ag NPs are cytotoxic [16–18] i.e. they cause cell membrane damage [19], DNA damage [20], oxidative stress [21], and the formation of reactive oxygen species (ROS) [22]. *Staphylococcus aureus* (*S. aureus*) is the most common type of bacterium that causes skin infection [23,24]. As the first generation of glycopeptide antibiotic, vancomycin has been demonstrated to possess remarkable bactericidal properties, especially against *S. aureus*. It interferes with the synthesis of the cell wall of the bacteria by disturbing the peptidoglycan molecules [25], which are key components in the cell wall structure, and then inhibit the generation of phospholipids and polypeptides. Especially, the use of these antibiotics, alone or combined with other antibiotics, does not induce cross-resistance [9]. Therefore, vancomycin has become the preferred antimicrobial agent for the treatment of contaminated wounds. Recently, Hsu et al. [7] developed a biodegradable composite film loaded with thrombin and vancomycin and observed instant hemostasis and effective antibacterial effects. However, few surgical dressings are compatible with acute irregularity wounds [9].

Extracellular matrix (ECM) hydrogel is a promising regenerative material that can effectively promote the repair of tissue defects. As previously reported [51], the entire ECM contains proteoglycans, growth factors, and matricellular proteins, including collagens, elastin, laminin, fibronectin, hyaluronan, heparan, basic fibroblast growth factor (bFGF), vascular endothelial growth factor (VEGF), and thrombospondin. Among them, a major component of ECM is collagen. ECM hydrogel formation is a collagen-based self-assembly process that is regulated in part by the presence of glycosaminoglycans, proteoglycans, and ECM proteins [52]. Furthermore, Kim, B young Soo et al. [55] formulated decellularized porcine skin as a printable bio-ink, and engineered a perfusable and vascularized 3D human skin equivalent composed of epidermis, dermis, and hypodermis with this bio-ink. The four compartments (epidermis, dermis, hypodermis, and blood vessels) were successfully matured under polycaprolactone (PCL)-based printed platform, indicating that extracellular matrix of skin can promote skin regeneration and wound healing. As the ECM hydrogels derived form porcine skin possesses good plasticity, injectability, biocompatibility and renewability, it can be applied to irregular skin tissue injuries and accelerate tissue healing [26–29]. Moreover, ECM is closely related to thrombosis [30]; under certain physiological conditions, the exposure of subcutaneous ECM and the subsequent platelet accumulation influence the control of hemorrhage [31–33]. Thus, ECM proteins (including fibrin, fibronectin, collagen, etc.) can effectively control bleeding. However, few studies have been applied to hemostasis. Recently, Hu et al. designed a nanocomposite hydrogel based on an acellular cardiac extracellular matrix (ECM) for vascular embolization, a wide range of miniature and standard clinical catheters are available that can swiftly inject the hydrogel into the wound and cause hemostasis, which has been published in Adv. Mater [34]. Therefore, ECM hydrogels is a relative new point to be applied in hemostasis application. These characteristics show that ECM hydrogels can control active bleeding by promoting thrombosis and can be utilized for irregular wounds to effectively control hemorrhage and accelerate healing [26–34]. Despite these advantages, ECM hydrogels still lack antimicrobial functionality. Moreover, in some situations, ECM hydrogels may act as a natural breeding ground for bacteria, especially in the case of wound contamination, which leads to bacterial infection [35,36]. Therefore, antibacterial ECM hydrogels are important for wound repair.

Recently, vancomycin-loaded biomaterials have been used to sterilize the wound and prevent bacterial infections [9,37,38]. Most studies focused on loading vancomycin on the biomaterials by covalent modification to release the antibacterial agent in a slow and steady manner to achieve a sustained bactericidal effect [39–41]. However, owing to the inadequate early release rate of antibacterial drugs in acute contaminated wounds, this approach may not always achieve sufficient antibacterial effects. Residual bacteria can reach all the organs in the body from the damaged blood vessels through the blood channel, causing secondary infections including infective endocarditis, lung abscess, and liver abscess [42]. Compared to the direct application of vancomycin powder and vancomycin solution, the VADM hydrogel has the following advantages: (1) The content of vancomycin released from VADM hydrogel is less than direct application, which not easy to produce drug resistance [53] and cytotoxicity [48]; (2) VADM hydrogel can adhere tightly to the wound, form a physical barrier against bacteria around the skin, and can absorb exudates, help remove necrotic tissue, prevent excessive loss of body fluid, form a low oxygen microenvironment for wound healing [35]. Therefore, a non-covalent combination of biomaterials and vancomycin should be conducive to the burst and rapid release of the agent in acute wound infections, rapidly exterminating the bacteria and reducing the rate of spread of infection before systematic treatment [43–45].

In this study, we designed a multifunctional porcine-skin ECM hydrogel with antimicrobial properties and effective bleeding control with vancomycin as an antimicrobial agent that non-covalently bonds with the porcine skin ECM hydrogel. The physicochemical properties, cytotoxicity, and wound-healing efficiency of antibacterial hydrogels were scrutinized. The hemostatic ability of hydrogels and the influence of vancomycin content on their bactericidal effect were systematically investigated to obtain the best composition of the hydrogel–anti-bacterial drug system suitable for application in acute wounds. Sprague-Dawley (SD) rats were selected as our experimental animals as Zhang Xiao-Na's report [54], in which the rats were used as streptozotocin-induced diabetic models to assess the role of Angelica dahurica ethanolic extract (ADEE) treatment on accelerating healing of diabetic wounds. The results demonstrated the potential of the hydrogel as a wound-dressing material for bactericide and acute hemorrhage control.

2. Materials and methods

2.1. Materials

Vancomycin was purchased from Aladdin (Shanghai, China), Triton X100 and $CH_3(CH_2)_{11}SO_4Na$ from Sinopharm Chemical Reagent Co., Ltd. (China), Pig glycosaminoglycan (GAG) ELISA Kit from Jianglai Biotechnology Co., Ltd (Shanghai China), Hyp assay kit from Beijing solarbio science & technology Co., Ltd. (China). Agar from Sangon Biotech Co., Ltd. (Shanghai, China), TRYPTONE from OXOID (Shanghai, China), and soya peptone from Sinopharm Chemical Reagent Co., Ltd. (China). DNA kit from CW Biotech (Beijing, China), Live/dead cell staining dye was purchased from BioVision (USA), and Cell Counting Kit-8 (CCK8) from APExBIO Technology LLC (USA).

2.2. Preparation of porcine acellular dermal matrix hydrogel

Fresh porcine skin was obtained from a local abattoir. After cleaning the cadaver, removing the subdermal fat tissue and hair, the tissues were rinsed thrice with sterile water and subjected to freeze–thaw (–80 to 37°C) cycles for three consecutive times. At 120 rpm and constant temperature (25°C), the tissues were treated with 1% Triton X-100 solution (Sinopharm Chemical Reagent Co., Ltd., China) for 12 h and 1% $CH_3(CH_2)_{11}SO_4Na$ (Sinopharm Chemical Reagent Co., Ltd., China) for 6 h. The resulting acellular dermal matrix (ADM) tissues were washed by phosphate-buffered saline (PBS) for several times and freeze-dried

overnight. Then those samples were milled to a powder (i.e. ADM) and digested by high-quality pepsin powder in a dilute HCL solution (pH 2–3) containing different concentrations of vancomycin for 6 h. The osmotic pressure was adjusted by dropping 40X PBS buffer, and the pH was adjusted to 7.2–7.4 by gradual dropwise addition of 10-M sodium hydroxide (NaOH) cooled beforehand. These steps were performed aseptically. Five samples of the skin were separately prepared in the following compositions: (1). Porcine ADM hydrogel; (2). Porcine ADM hydrogel containing 1 mg/mL vancomycin (represented as VADM1); (3). VADM2; (4). VADM4; and, (5). VADM6. The pH-adjusted formative gel can be stored at 4°C for up to 1 week.

2.3. Characterization of porcine acellular dermal matrix materials

We used hematoxylin and eosin (H&E) and 4′, 6-diamidino-2-phenylindole (DAPI) stains and a DNA assay to evaluate the cellular and nuclear removal efficacies. DNA was extracted with a Universal Genomic DNA kit and its concentration was determined from the absorbance at 260 nm on a microplate spectrophotometer. The GAG content of native and decellularized tissue was quantified using the Pig glycosaminoglycan (GAG) ELISA Kit and collagen content was measured with a hydroxyproline (HYP) assay kit.

The nanofibrous structures of the ADM and VADM hydrogels could be examined by scanning electron microscopy (SEM). After solidification, Hydrogels from each group were fixed in 2.5% (w/v) glutaraldehyde for an hour. Then, the samples were washed with PBS solution thrice (10 min per wash cycle). Subsequently, they were again washed thrice with PBS for 5 min each, and then dehydrated by sequential treatment with 30%, 40%, 50%, 70%, 80%, 90%, 95%, and 100% CH_3CH_2OH (10 min for each gradient). After the treatment, the samples were dehydrated at a critical point dryer with liquid CO_2. Finally, they were sputter-coated with Au–Pd and observed under SEM (JSM-6360LV, JEOL, Tokyo, Japan). Energy-dispersive spectrometry analysis (X-Act, OXFORD, British) was performed to study the chemical composition of the interface.

2.4. Diffusion of antibiotic (zone of inhibition)

The zone of inhibition (ZOI) is a circular area around the region of an antibiotic in which the bacteria colonies do not grow. The inhibitory effects of the five hydrogels were measured using the Oxford cup method. *S. aureus* and *Enterococcus* (control group) were cultured in Luria-Bertani (LB) medium containing tryptone (15 g/L) and peptone from soya (5 g/L) at 37 °C overnight. Inhibition zone assay was performed using the agar diffusion method (the Oxford cup method). Briefly, 15 g/L of LB agar was used as the solid medium, sterilized, and heated until it melted. The melt was then poured into 90-mm-diameter Petri dishes, 15 mL per dish (lower layer), and allowed to solidify. Oxford cups with an inner diameter of 6 mm each were placed in the center of the agar plates. The molten LB agar medium was then cooled to approximately 50 °C and mixed with the test bacteria. Subsequently, 5 mL of the molten LB agar contain with bacteria was added to the solidified medium (lower layer) and allowed to coagulate and form the upper layer. After the coagulation process, the Oxford cup was removed, a well could be left in the solid medium, and then the hydrogel sample (ADM, VADM1, VADM2, VADM4, VADM6) was added to the well. After 16–18 h of incubation, the zone of inhibition (ZOI) was estimated by subtracting the diameter of the hydrogel cylinder from the diameter of the inhibition zone. .

2.5. Antibacterial activity test

Considering that the experimental group was loaded with gradient concentrations of vancomycin as an intervention measure, we chose untreated acellular pig skin gel as the control group. The experimental design was based on previous reports [37]. To compare the bactericidal effect of the materials, we first studied the relationship between the bacterial dilution ratio and the optical density (OD) value (600 nm). After centrifugation, the samples at 5000 rpm for 5 min, we removed the supernatant and suspended *S. aureus* in normal saline (NS). The bacterial suspension (100 μL) was transferred to a 96 well UV–visible-transparent plate, and the absorbance was measured at an OD of 600 nm using a UV spectrophotometer. The OD value was measured again after diluting the bacterial suspension with NS, and the standard curve of OD vs. dilution ratio was plotted.

The antibacterial activity of the hydrogels against *S. aureus* was investigated according to a previous study with slight modifications [37]. First, the ADM and VADM hydrogels (0.3 mL each) were placed in 2-mL Eppendorf tubes, 0.5 mL of the bacterial suspension was added, the *OD* value was measured, and then the mixture was incubated at 37°C for 12 h. After incubation for 12h, the bacterial suspension was centrifuged at 5000 rpm for 5 min. After removing the supernatant, the bacteria were suspended in NS. The bacterial suspension (100 μL) was transferred to a 96 well UV–visible transparent plate, and the absorbance was measured at an OD of 600 nm using a UV spectrophotometer. The residual bacterial suspension was serially diluted, placed on agar plates, and measured after being incubated for 24 h. The antibacterial ratio of the planktonic bacteria (*Rap*) was calculated according to the equation: $Rap\ (\%) = ([A - B]/A) \times 100\%$, where A and B represent the number of viable bacteria in the control group (ADM hydrogel) and experimental group (VADM hydrogel), respectively.

2.6. In vitro release kinetics of vancomycin from hydrogels

First, the absorbance of the solution at different vancomycin concentrations was measured at an OD of 281 nm, and the standard curve between the vancomycin concentration and absorbance was plotted. 100 μL of VADM1, VADM2, VADM4, and VADM6 were prepared in an Eppendorf tube (2 mL). 1 mL of phosphate buffer (pH 6) was added after solidifying the hydrogels at 37 °C. Then, hydrogels with the added buffer were steadily stirred at 37°C. The buffer solution was collected and centrifuged at 3000 rpm for 5 min to homogenize it. 100 μL of the solution was transferred to a 96 well UV–visible transparent plate, and the absorbance was measured in duplicate at an OD of 281 nm using a UV spectrophotometer. The absorbance was measured for 120 min in 10-min intervals. The concentration of the released vancomycin was determined, and the vancomycin release rates of VADM1, VADM2, VADM4, and VADM6 were calculated according to the standard curve of vancomycin.

2.7. Hemolytic activity

Liu et al. was referred for information on the hemolytic activities of the antibiotic-loaded hydrogels [46]. The gels were prepared in 2-mL Eppendorf tubes. Red blood cells (RBCs) obtained from a healthy donor were isolated by centrifugation at 1000 rpm for 10 min, and diluted in NS (volume ratio, 4/5). Then, a 0.2-mL RBC suspension was mixed with 5 mL of the NS (negative group), 5 mL of distilled water (positive group), and hydrogels. The mixtures were incubated for 60 min at 37°C, and then centrifuged at 3000 rpm for 5 min. The supernatant was carefully removed and transferred to a 96 well plate. The OD was determined by spectroscopy at an OD of 540 nm. The hemolysis ratio was calculated by the hemolysis ratio $(\%) = \{([\text{experiment group (OD)} - \text{negative group (OD)}]) / ([\text{positive group (OD)} - [\text{negative group (OD)}])\} \times 100\%$; where OD = 540 nm.

2.8. Cell viability determined by live/dead assay

Hydrogels were prepared in a six well plate with a volume of 500 μL and sterilized before use. The mouse embryonic cells (NIH3T3 cells) were seeded in the ADM and VADM hydrogel-coated wells at a density of 4×10^4 cells per well. Dulbecco's Modified Eagle Medium (DMEM, Hyclone) with 10% (v/v) FBS, 100 μg/mL penicillin, and 100 μg/mL streptomycin were added. The cells were incubated in a humidified atmosphere containing 5% CO_2 at 37°C. At time periods determined beforehand, the cells were stained using a the live/dead cell stain kit and

observed under a fluorescence microscope.

2.9. Cytotoxicity of hydrogel against NIH3T3 cell line

Cytotoxicity was determined using the Cell Counting Kit-8 (CCK8) (APExBIO Technology LLC, USA). The ADM and VADM hydrogels were immersed in DMEM (volume of hydrogel/volume of medium = 1:5) at 37 °C for 24 h. Collected the supernatant extract as the 100% leaching solution, then mixed with a certain proportion of DMEM medium to obtain 0%, 25% 50%, 75% leaching solution for further experiments. The NIH3T3 cells were seeded in a 96 well plate at a density of 3000 cells per well. After incubation at 37 °C for 24 h, the supernatant medium was removed from each well and 100 μL graded concentrations of leaching solution were added (0%, 25%, 50%, 75%, 100%, n = 5 for each concentration per day) for 1, 3, and 5 days. The NIH3T3 cells cultured with DMEM (0% leaching solution) was the control group. Subsequently, 10 μL of the CCK8 reagent was added to each well and quantified the cell metabolism after incubating for 1 h at 37 °C. The absorbance at an OD of 450 nm was measured using a spectrophotometer.

2.10. Dynamic coagulation test

The ability of the hydrogels to clot whole blood was tested according to a method reported in the literature with slight modifications [47]. First, 300 μL of the hydrogel was added to a 24 well plate and incubated for 10 min at 37°C to allow gel solidification. Ten microliters of a recalcified whole-blood solution (0.2 M calcium chloride [$CaCl_2$], 1 μL in blood) was added to the hydrogels in the 24 well plate. The well was incubated at 37 °C for 30, 60, 90, 120, 150s and 180 s. The gelatin sponge and gauze were used as control groups for comparison with the hydrogel. After the period set beforehand, 2 mL of de-ionized water was gradually added to release unbound blood without disturbing the clot. The absorbance of the supernatant was measured at an OD of 545 nm using a spectrophotometer. All experiments were repeated three times. The absorbance of 10 μL of recalcified whole blood in 2 mL of de-ionized water was used as the negative control. The blood-clotting index (BCI) was calculated according to the formula: BCI% $= ([A - C]/[B - C]) \times 100\%$, where A is the absorbance of the hydrogel, B the absorbance of the negative control, and C the absorbance of de-ionized water.

2.11. Rat liver and kidney laceration

Healthy male Sprague-Dawley (SD) rats purchased from the experimental animal center of Zhejiang Academy of Medical Sciences were fed in a controlled environment with constant temperature (22–25°C) and humidity (50–60%) for 1 week with food and water available. Six SD rats (300–400 g, 8 weeks) were used as test subjects in a series of experiments. Those rats were anesthetized with 10% chloral hydrate for 2 min before surgery (intraperitoneal injection, chloral hydrate 10%/rat body weight = 0.5 mL/100 g). The first was the rat liver laceration experiment. The abdominal cavity of the rat was gently cut open with surgical scissors to fully expose the liver. Serous fluid around the livers was carefully removed for the accurate assessment of blood loss. Thereafter, an incision (length = 1 cm and depth = 0.3 cm) was cut in the livers of three rats with a surgical scalpel. The VADM hydrogel (2 mL) and gauze were placed over the wound, while the other group without treatment was used as control. When the Bleeding stopped, the blood loss was weighed. The second was the rat renal-tissue-defect experiment. The abdominal cavity of the rat was gently cut open with surgical scissors to fully expose the kidney. A cylindrical wound with a diameter of 1 cm and a depth of 0.5 cm was incised into the tissue of three rats with tissue scissors. Then, The VADM hydrogel (1 mL) and gauze were placed over the wound, while the other group without treatment was used as control. When the Bleeding stopped, the blood loss was weighed. Tissues around the liver and kidney incision treated with VADM hydrogel were collected for hematoxylin and eosin (H&E) analysis to further explore the mechanism of hemostasis.

2.12. Rat abdominal aorta hemostasis tests

Four SD rats weighing 300–400 g were chosen for the aortic hemostasis test. Those rats were anesthetized with 10% chloral hydrate for 2 min before surgery (intraperitoneal injection, chloral hydrate 10%/rat body weight = 0.5 mL/100 g). The abdominal cavity of the rat was gently cut open with surgical scissors to fully expose the abdominal aorta. Then the abdominal aorta was peeled from the surrounding tissues and clamped using hemostatic forceps, and subsequently clipped using surgical scissors. The hydrogels (0.2 mL) were applied to the hemorrhaging site. After 5 min of gelation, the forceps were removed, and the site was visually inspected to determine if the bleeding had stopped. The control group did not use the hydrogel, and the bleeding continued even after 5 min. The abdominal aorta treated with VADM hydrogel were collected for hematoxylin and eosin (H&E) analysis to further explore the mechanism of hemostasis.

2.13. In vivo healing of S. aureus infected wounds by hydrogels

The SD rat model was established based on a previously reported method [46]. Based on the application of vancomycin hydrogel with different concentrations, the healing rate of infected incisions in SD rats demonstrated different results. Ten Rats (weight ∼ 300g) were randomly into two groups: one group was treated for 1 week, and other for 2 weeks. Those rats were anesthetized by intraperitoneal injection of chloral hydrate (10%, 0.5 mL per 100 g of body weight). Once the rats were fully anesthetized, their dorsal hair was shaved to form an area of approximately 8 × 8 cm². After disinfecting it with 75% alcohol, a round full-thickness skin incision with a diameter of 1 cm was made on the dorsal skin. A *S. aureus* suspension (1×10^7 CFU/mL) was administered to the round skin wounds and then dried for 2 h. Subsequently, the ADM or VADM hydrogel was applied to the infected wounds, whereas the untreated wounds were used as negative controls. The area of the wound was measured at time periods set beforehand after treatment. Wound closure was calculated by the following equation: wound closure rate (%) $= ([W_0 - W_n]/W_0) \times 100\%$, where W_0 and W_n represent the wound area at day 0 and the sampling time, respectively. The H&E stain was used to evaluate the wound-healing process. To distinguish infiltrated inflammatory cells from the infected wound, formalin-fixed wound was used for the CD68 stain and myeloperoxidase (MPO) stain.

2.14. Statistical analysis

Data are presented as the mean ± standard deviation. Data were analyzed by one way analysis of variance with graphpad prism7 (Graphpad Software Inc., USA). The sample size (n) for each statistical analysis has been reported in the corresponding 'experimental section' and 'figure legends' and significance was defined as $p < 0.05$.

2.15. Ethics approval

Animal experiments were carried out in the experimental animal center of Zhejiang Academy of Medical Sciences. All animal studies were conducted in accordance with the National Institutes of Health Guidelines and guidelines for the care and use of experimental animals of Zhejiang Academy of Medical Sciences.

3. Results and discussion

3.1. Hydrogel synthesis and characterization

After decellularization, a histological analysis was performed to assess the completeness of decellularization and the integrity of the extracellular matrix. According to the H&E stain results, cell nuclei were

absent, and the ECM remained intact after decellularization (Fig. 1a–b). The DAPI staining revealed no staining nuclei in the acellular tissues (Fig. 1c–d). These results prove that the entire extracellular matrix structure of the porcine dermal tissue is preserved after decellularization. DNA quantification also revealed a significant decrease in DNA content compared to that of native tissue: porcine dermal tissue (753.5 $\pm$ 143.6 ng/mg dry weight vs. 11.83 $\pm$ 3.74, $p < 0.05$, Fig. 1k). Collagen content quantification (Fig. 1k) revealed no significant change in the porcine dermal tissue (389.4 $\pm$ 32.39 ng/mg dry weight vs. 373 $\pm$ 26.79, $p > 0.05$, Fig. 1k). Pig glycosaminoglycan (GAG) quantification revealed a significant decrease in GAG content compared to that of native tissue: porcine dermal tissue (0.26 $\pm$ 0.01 µg/mg dry weight vs. 0.22 $\pm$ 0.01, $p < 0.05$, Fig. 1k). Liquid N_2 and ADM, VADM1, VADM2,

VADM4, and VADM6 were added to the decellularized porcine dermal tissue. The tissue was ground into powder using TissueLyser (Jingxin, Shanghai) and the hydrogels were made with different concentration vancomycin (Fig. 1e–g). As shown in Fig. 1h, the resulting gel solution was incubated at 37°C for 5 min and then transformed from the solution (liquid) state into a homogeneous, translucent gel (solid) state. The potential mechanism of gel forming process may be as described by Kadler Karl E [57]. The GAGs cause the collagen to gel faster and form larger fibers, while the proteoglycans cause the collagen to gel faster. Scanning electron microscopy (SEM) revealed nanofibrous networks in the hydrogel scaffolds (Fig. 1i), which is beneficial for the adsorption of antibiotics. The compositions of different elements present in the hydrogels were studied using the energy-dispersive spectrometry (EDS)
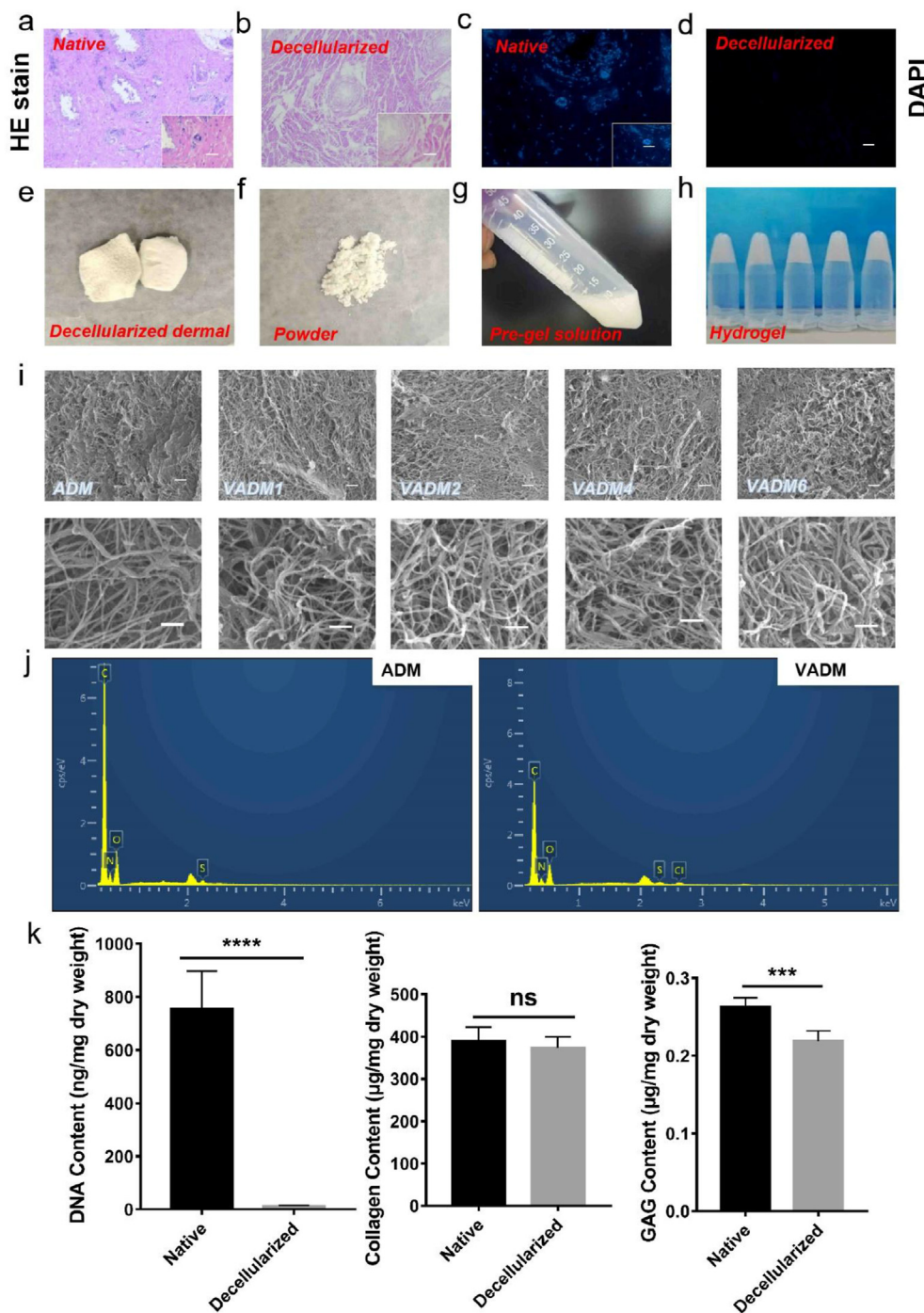

Fig. 1. Fabrication and characterization of hydrogel derived from porcine acellular dermal matrix (ADM). (a–d) H&E and DAPI stains confirm decellularization. Scale bar = 100 µm. (e–h) Porcine ADM and hydrogel preparation. (i) SEM analysis of the nanofibrous structures of ADM and VADM (vancomycin 1 mg/mL·, 2 mg/mL, 4 mg/mL, and 6 mg/mL) at various magnifications. Scale bar = 1 µm. (j) Energy-dispersive spectrometry image analysis of chemical elements on surfaces of ADM and VADM. (k) Quantitative testing of DNA (n = 5), collagen (n = 5) and GAG (n = 5).

system. The ADM hydrogels dehydrated by an ethanol (CH_3CH_2OH) gradient no longer contained Cl element, whereas the VADM hydrogels did, which contain $0.11 \pm 0.07\%$, albeit in small quantities (Fig. 1j). The Cl element content comes from vancomycin hydrochloride and can strongly bond with the extracellular matrix hydrogel, making rinsing or dehydration ineffective in debonding it.

3.2. In vitro antibacterial activity

As *Staphylococcus aureus* is responsible for most skin infections, we tested the antibacterial performance of the vancomycin-loaded hydrogel against an *S. aureus* suspension. This suspension was diluted multiple times, and the optical density (OD) values at 600 nm were measured. The results demonstrate a power function relationship between the OD value of *S. aureus* and the dilution ratio (Fig. 2a), which was demonstrated by Lambert Beer's law [58]. This, in turn, indicates that the antibacterial efficacy of hydrogels can be evaluated by comparing the OD values of *S. aureus* for the five hydrogel concentrations. The hydrogels (porcine acellular dermal matrix hydrogel [ADM], porcine ADM hydrogel with vancomycin group 1 [VADM1], VADM2, VADM4, and VADM6) were prepared in 2-mL Eppendorf tubes and then co-cultured with a 1-mL *S. aureus* suspension at 37°C for 12 h to measure the OD value. The results revealed a significant increase in the OD value of the ADM group, but the opposite trend in those of the VADM1, VADM2, VADM4, and VADM6 groups. A notable fact is that the downward trend of the OD value between the VADM2, VADM4, and VADM6 groups demonstrated no significant changes, which may be attributed to the following two reasons: one is that the concentration of bacteria in the solution exceeds the applicable range of Lambert Beer's law, and the other is that the concentration of bacteria in the solution is indeed not of significant difference, because when vancomycin released from the material exceeds the minimum inhibitory concentration (MIC, $20\mu g/mL$ [59]), all bacteria would be killed, indicating they exhibit similar antimicrobial effects (Fig. 2b).

To further evaluate the bactericidal behavior of the VADM hydrogels, we measured the antiplanktonic bacteria rate by a plate colony-formation assay. Numerous colonies of bacteria belonging to the ADM group had grown on the agar plate (Fig. 2cA1), whereas those belonging to VADM1, VADM2, VADM4, and VADM6 decreased significantly (Fig. 2cA2-5).

These results indicate that the VADM groups can kill *S. aureus*. The antiplanktonic bacteria ratio (Rap) of VADM1, VADM2, VADM4, and VADM6 were $86.48 \pm 0.38\%$, $95.86 \pm 0.68\%$, $97.34 \pm 0.79\%$, $98.09 \pm 0.73\%$, respectively. The antiplanktonic bacteria rate of the VADM hydrogel groups increased steadily with an increase in the vancomycin concentration (Fig. 2d). However, when the concentration of vancomycin exceed 2 mg/mL, the Rap was not of statistical significance ($p > 0.05$). Therefore, high vancomycin antibacterial loads are not required to stop the spread of infection in traumatic injuries. This in turn may further reduce the cytotoxicity caused by high vancomycin concentrations [48,49].

3.3. Zone of inhibition experiment

The antibacterial activity effect was evaluated on both Gram-negative (*Enterococcus*) and Gram-positive (*S. Aureus*) bacterium. As for infected wounds, the bacterials usually colonize the wound surface and easily invade deep tissues, causing a series of pathophysiological changes [50]. A zone of inhibition (ZOI) experiment was performed to determine the bactericidal effect of vancomycin ejected by the VADM hydrogels in deep tissues. The ADM hydrogel did not form any ZOI against *S. aureus* because it did not contain vancomycin (Fig. 3a). However, VADM1, VADM2, VADM4, and VADM6 formed significant ZOI against the *Enterococcus* and *S. aureus* lawns grown on the agar plate, thereby indicating the diffusion of the agent into the surroundings that deactivated bacteria in those areas (Fig. 3a). The VADM6 group possessed the largest ZOI because it had the highest content of vancomycin. The VADM1 group formed the smallest ZOI with the least amount of vancomycin (Fig. 3b). These results indicate a clear relationship between ZOI and vancomycin concentration, which is consistent with the results of previous studies [37]. However, the antimicrobial activity between *Enterococcus* and *S. aureus* were no significant difference ($p > 0.05$).

3.4. In vitro drug release study

Pre-hospital trauma wounds are vulnerable to a variety of bacterial infections, ranging from superficial skin infections to more severe invasive diseases including endocarditis, osteomyelitis, and septicemia. Therefore, this study used an extracellular matrix hydrogel to absorb
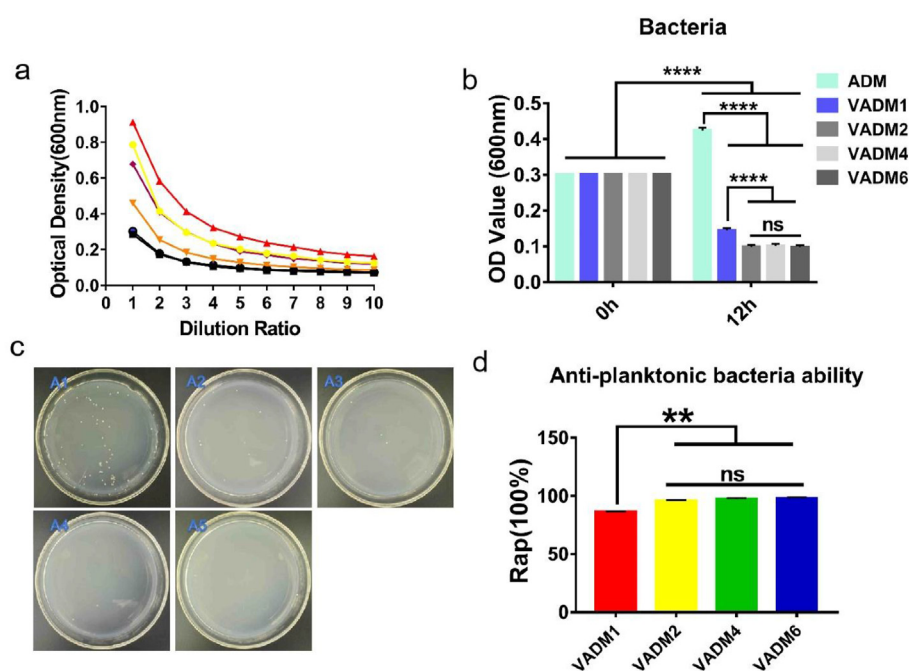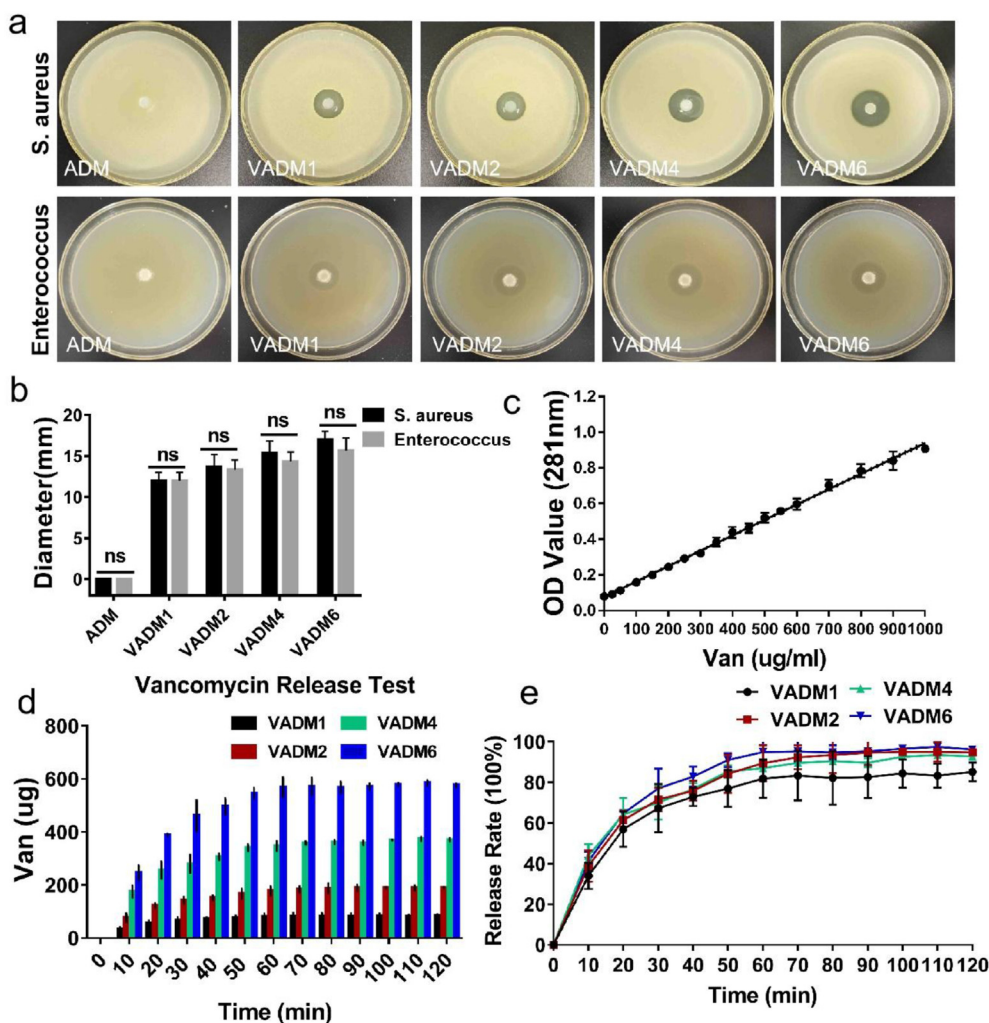

Fig. 2. *In vitro* antibacterial activity of ADM and VADM hydrogels. (a) Relationship between dilution ratio and absorbance of *S. aureus* (six groups with different initial absorbances). (b) Absorbance of *S. aureus* suspension co-cultivated with different hydrogels before and after 12 h. ADM hydrogel is the control group. (c,d) Bacterial counts of *S. aureus* suspension by the spread-plate method after co-cultivation with different hydrogels for 12 h and quantitative analysis. A1–A5 represent ADM, VADM1, VADM2, VADM4, and VADM6, respectively. Scale bar = 1 mm. Every kind of hydrogels were tested for three times and the data are represented as mean $\pm$ SD. Significant differences are indicated as ns ($p > 0.05$), * ($p < 0.05$), ** ($p < 0.01$), *** ($p < 0.001$), or **** ($p < 0.0001$). *Rap*: antiplanktonic bacteria ratio.

Fig. 3. Diffusion and release of vancomycin from the hydrogels. (a) Each plate has a confluent lawn of *S. aureus* or *Enterococcus* where the vancomycin diffuses from the central hydrogel disc and kills the surrounding bacteria, leaving a clear zone. Scale bar = 10 mm. (b) Zone of inhibition (ZOI) quantitative analysis of VADM and ADM (control group) against *S. aureus* and *Enterococcus*. (c) Relationship between concentration of vancomycin and absorbance at OD281 value (n = 10). (d) Amount of vancomycin released from VADM1, VADM2, VADM4, and VADM6, respectively, at different time intervals. Initially, the hydrogels contain 100, 200, 400, and 600 μg of vancomycin and are used to study release kinetics by adding 1 mL of PBS buffer solution (pH = 6). The amount of vancomycin content in the solution is then determined by UV–visible absorption spectroscopy. (e) Vancomycin release rates of VADM1, VADM2, VADM4, and VADM6, respectively in PBS buffer (pH = 6). Every kind of hydrogels were tested for four times and the Date are presented as mean ± SD, ns ($p > 0.05$), * ($p < 0.05$), ** ($p < 0.01$), *** ($p < 0.001$), or **** ($p < 0.0001$).

significant amounts of vancomycin and enable rapid bactericide through explosive release, which is crucial in care before hospitalization. The amount of vancomycin released was determined by measuring the absorbance using a UV spectrophotometer. Four VADM hydrogels (100 μL) were prepared in 2-mL Eppendorf tubes. VADM1, VADM2, VADM4, and VADM6 contained 100, 200, 400, and 600 μg of vancomycin, respectively. Related studies have shown that the acidic environment of infected wounds originates from an insufficient supply of nutrients and oxygen, and increased glycolysis [35]. Meanwhile, in our previous study, the muscle tissue in infected rats was homogenized, and the pH value of the supernatant as measured by blood gas analysis was 6.1 ± 0.6, which confirmed the acidic microenvironment under the infected state [40]. Therefore, in this study, we investigated the release kinetics of vancomycin in a phosphate-buffered saline (PBS) solution at pH = 6. Fig. 3c indicates a linear relationship between the vancomycin concentration and the absorbance at 281 nm. Hence, the concentration of vancomycin can be estimated based on its OD value. As shown in Fig. 3d, at an hour, the amount of vancomycin released from VADM1, VADM2, VADM4 and VADM6 were 81.85 ± 9.45, 178.89 ± 17.64, 348.15 ± 17.58, 569.63 ± 36.35 μg, respectively and the release rate of vancomycin from VADM1, VADM2, VADM4 and VADM6 were 81.85 ± 9.45%, 89.44 ± 8.82%, 87.04 ± 4.40%, 94.94 ± 6.06%, respectively (Fig. 3e). The vancomycin release was detectable in the laboratory for up to 9 h. These results proved that the hydrogel can expeditiously eject vancomycin in acute contaminated wounds to create a relatively sterile environment, which is of great significance in the prevention of infection in emergency treatment before hospitalization.

3.5. Biocompatibility

Vancomycin has demonstrated a strong bactericidal effect on gram-positive bacteria, mainly by inhibiting the synthesis of bacterial cell walls. However, in high concentrations, vancomycin is cytotoxic [48,49]. Therefore, the compatibility of the ADM and VADM hydrogels *in vitro* with human RBCs (hRBCs) was investigated. The hRBCs were directly exposed to the surfaces of ADM and VADM hydrogels, and the hemolysis rate was calculated to evaluate the blood compatibility of the hydrogels. The vancomycin-loaded hydrogels (VADM1, VADM2, VADM4, and VADM6) exhibited less than 3% hemolysis, which is negligible, similar to the ADM (Fig. 4a). Thus, the hydrogels are compatible with human erythrocytes.

Subsequently, the cytocompatibility of the VADM hydrogels by live/dead staining was evaluated. The hydrogels were then co-cultured with NIH3T3 cells. After one week, the results of the live/dead staining revealed living cells on the ADM and VADM hydrogels (Fig. 4b) without hydrogel-induced cytotoxicity. Further, the cell toxicity of the hydrogels was investigated by CCK-8 assay to measure the cell metabolic activity. Fig. 4c–d reveal no significant decrease in cell metabolic activity was observed between the control group (NIH3T3 cells cultured with DMEM) and other group (NIH3T3 cells cultured with 25%, 50%, 75% and 100% extraction DMEM of ADM and VADM1) on days 1, 3, or 5 (all $p > 0.05$). However, Fig. 4e–g shown in VADM2, VADM4, and VADM6, the cell metabolic activity was decreased obviously between the control group (NIH3T3 cells cultured with DMEM) and other group (NIH3T3 cells cultured with 100% extraction DMEM) on day 5 ($p < 0.0001$). The
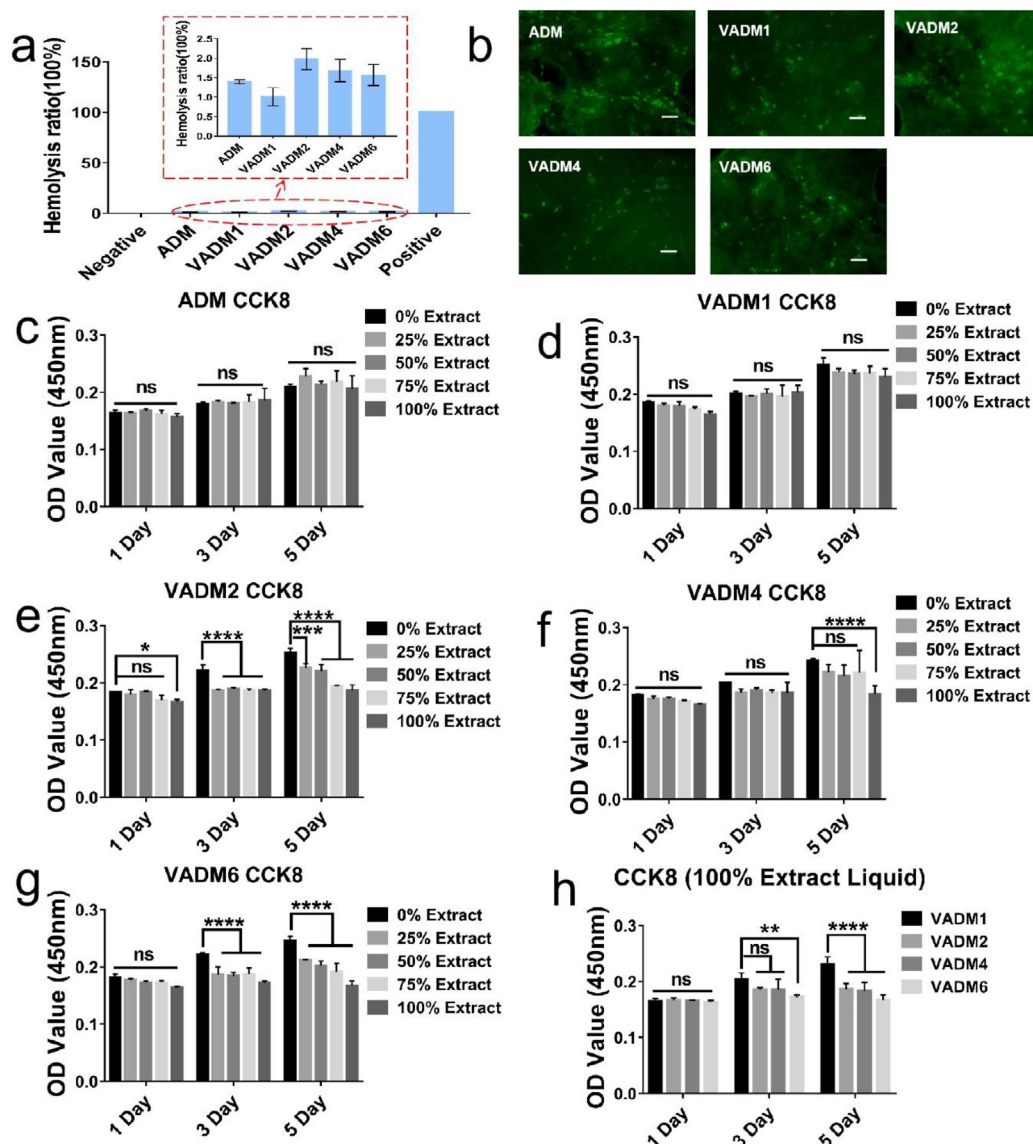
Fig. 4. *In vitro* experiments on biocompatibility and cytotoxicity. (a) hemolysis ratio of hydrogels with human RBCs. Normal saline (NS) solution and distilled water are the negative and positive controls, respectively. (b) Fluorescence microscopy images of NIH3T3 cells cultured on ADM and VADM (vancomycin 1 mg/mL, 2 mg/mL, 4 mg/mL, and 6 mg/mL) hydrogels after staining in the live/dead assay; green indicates live cells. Scale bar = 100 μm. (c–g) Metabolic activity of NIH3T3 cells cultured in the control group (NIH3T3 cells cultured with Dulbecco's Modified Eagle Medium [DMEM]) and other group (NIH3T3 cells cultured with 25%, 50%, 75% and 100% extraction DMEM, n = 5 for each concentration per day) on days 1, 3, and 5. (h) Metabolic activity of NIH3T3 cells cultured in 100% extract liquid on days 1, 3, and 5 between VADM1, VADM2, VADM4 and VADM6. Three replicates of each sample were tested and the data were shown as mean ± SD. ns ($p > 0.05$),* ($p < 0.05$), ** ($p < 0.01$), *** ($p < 0.001$), or **** ($p < 0.0001$).

NIH3T3 cell growth became more restrained with the increase in vancomycin concentration, the incubation time stretched, and the inhibition effect became more obvious (Fig. 4h). Nevertheless, the metabolic activity of NIH3T3 cells in the VADM1 group distinctly increased.

The vancomycin-loaded ADM hydrogels had a low hemolysis rate, which was not affected by vancomycin content. This demonstrates the blood compatibility of the VADM hydrogels. In terms of cytocompatibility, NIH3T3 cells survived on the VADM hydrogels by the live/dead staining assay, even in the VADM6 group (Fig. 4b). However, the CCK8 test indicated that the cytotoxicity gradually became severe with increasing vancomycin concentration. Therefore, VADM1 not only kills bacteria swiftly and effectively, but it is also more biocompatible than VADM2, VADM4, and VADM6.

3.6. Hemostasis experiments

A dynamic whole-blood clotting time test was performed to evaluate the coagulability of the VADM hydrogels. The higher the blood-clotting index of the hemoglobin solution, the slower the coagulation rate of the VADM hydrogels. The hemostatic gauze and gelatin sponge were used as the control groups. As shown in Fig. 5aA1, the blood-clotting index of the gelatin sponge, gauze, ADM, VADM1, VADM2, VADM4 and VADM6 were 17.68 ± 1.37%, 10.03 ± 1.65%, 8.97 ± 0.79%, 8.44 ± 0.46%, 6.07 ± 2.29%, 4.48 ± 1.83% and 6.86 ± 2.78% at 180s, respectively. This indicates the VADM hydrogels have good coagulability. Fig. 5aA2 showed the coagulation ability of VADM1 hydrogel was significantly better than gelatin sponge ($p < 0.05$). After 90s, the
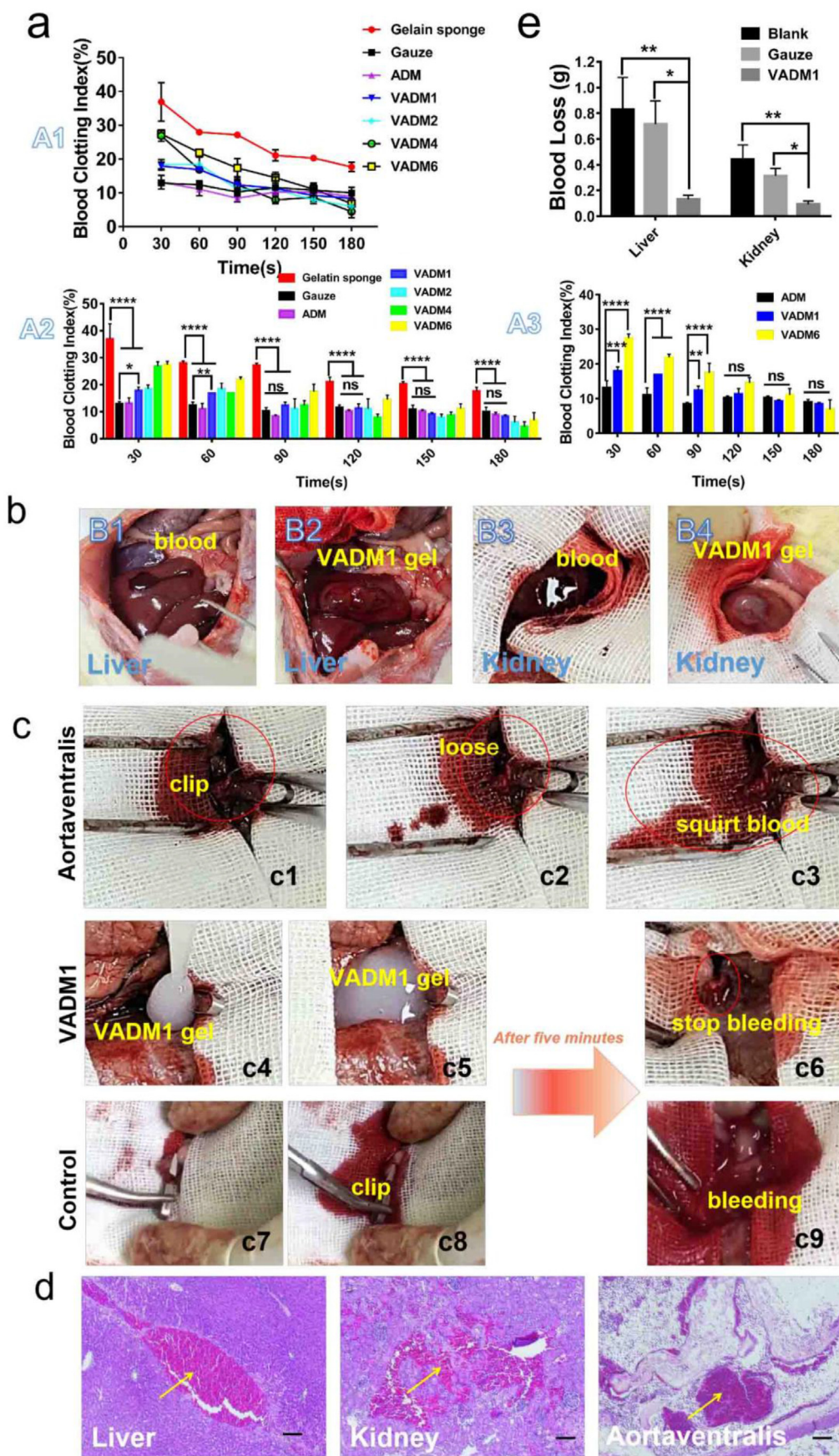
Fig. 5. *In vitro* and *in vivo* hemostasis test. (a) *In vitro* dynamic whole-blood clotting evaluation (A1, A2 and A3) of the ADM, VADM1, VADM2, VADM4 and VADM6 hydrogels, with gelatin sponge and gauze used as the control. (b) Photographs captured during the liver laceration model and renal tissue-defect model. (B1) A wound with a length of 1 cm in the liver. (B2) VADM1 hydrogel formed *in situ* on the trauma injury. (B3) A small portion of the kidney tissue was removed with surgical scissors. (B4) VADM1 hydrogel formed *in situ* on the defective tissue. (c) Photographs captured during a hemostasis test on the abdominal aorta (highlighted by red circles and ellipses). (c1) Clipped abdominal aorta. (c2,c3) Arterial spurts can be observed after release of the artery clip. (c4) VADM1 hydrogel applied to the wound. (c5) Abdominal aorta surrounded by VADM1 hydrogel. (c6) Artery clip was removed after 5 min, and the bleeding was stopped completely. The abdominal aorta was clogged with hydrogel. (c7–c9) Arterial spurts still occur on the control group after 5 min, when the artery clip was released. (d) H&E stained micrographs, showing significant accumulation of red cells (yellow arrow) within the incision site. Scale bar = 100 μm. (e) Blood loss from liver and kidney incisions. Three replicates of each sample were tested and the data were shown as mean ± SD.
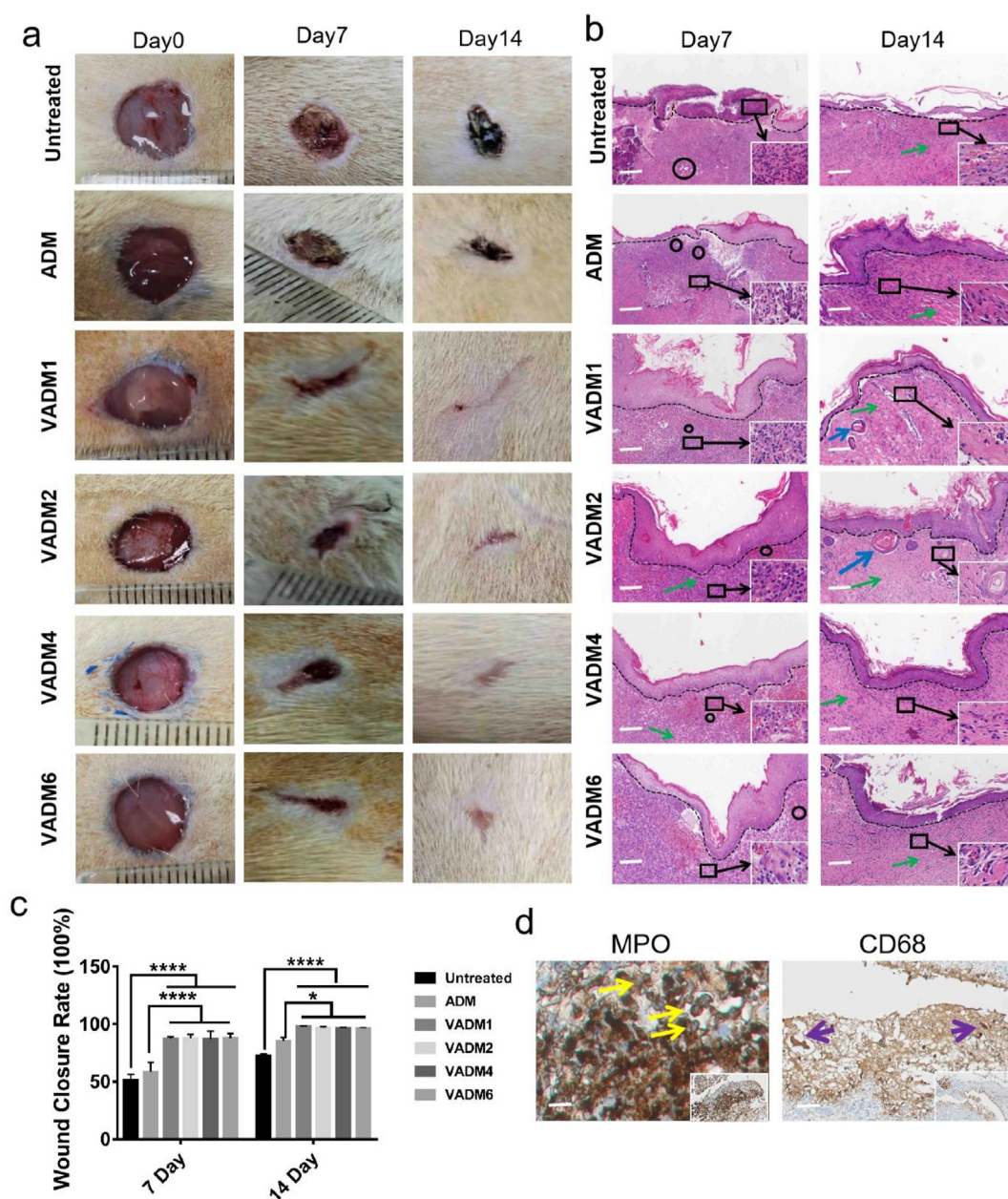
Fig. 6. *In vivo* wound-healing performance of hydrogels. (a) Photographs of wounds at determined days for untreated group, and ADM, VADM1, VADM2, VADM4, and VADM6 hydrogels. (b) H&E staining of wound sections in the control group, and groups treated with ADM, VADM1, VADM2, VADM4, and VADM6 hydrogels on days 7 and 14, respectively. Scale bar = 100 μm. All legends were represented as follows: Black box were inflammatory cells; black circles were vasculature; green arrows were myofibroblasts; blue arrows were hair follicles and black dashed lines were the boundary of epithelium and dermis. (c) Wound contraction for untreated group, and ADM, VADM1, VADM2, VADM4, and VADM6 hydrogels. Three replicates of each sample were tested and the data were shown as mean $\pm$ SD. ns (p > 0.05),* (p < 0.05), ** (p < 0.01), *** (p < 0.001), or **** (p < 0.0001). (d) Immunohistochemical staining of CD68$^+$ macrophages (purple arrow) and MPO-labeled neutrophils (yellow arrow). Scale bar = 100 μm.

coagulation ability of VADM1 hydrogel was no significant difference compared with gauze (*p* > 0.05). In Fig. 5aA3, with time prolonging, the coagulation ability of VADM1 and VADM6 was significantly enhanced. We speculated that vancomycin may enlarge the spatial structure of the extra-cellular matrix hydrogel. The net-like structure on the surface of VADM is looser than that of ADM, allowing more blood to penetrate into the structure and contact more collagen fiber, increasing the contact area of the blood and the hydrogel, thus leading to coagulation, which was similar to the report of Maas Coen's [56].

To further investigate the actual *in vitro* hemostatic capacity of the hydrogel on mammalian tissues, we used rat livers and kidneys to simulate hemorrhages. These results demonstrate that the VADM1

hydrogel is not only an effective bactericide, but also biocompatible. Therefore, we selected VADM1 for the subsequent animal experiments. The liver was lacerated using a surgical scalpel to induce incompressible bleeding (Fig. 5bB1). Then, we patched VADM1 to the incision, which stopped blood flow, achieving complete hemostasis (Fig. 5bB2). In liver incisions without treatment, 0.83 ± 0.25g of blood flowed onto the filter papers. The amount of blood loss in incisions with gauze and VADM1 was 0.71 ± 0.18g and 0.13 ± 0.03g, respectively. In renal tissue-defect model, we dissected part of the tissue with surgical scissors and allowed blood to continue to flow out of the incision (Fig. 5bB3). On filling injecting the tissue with VADM1, the hemorrhage stopped and no fresh blood flow could be detected (Fig. 5bB4). In renal tissue-defect without treatment,

0.44 ± 0.11g of blood flowed onto the filter papers, while that with gauze and VADM1 was 0.31 ± 0.06g and 0.09 ± 0.02g, respectively. The results from these models of the rat liver and kidney demonstrate the hemostatic effect of VADM1 on severe traumatic injuries.

To further study the hemostatic effect and mechanism of the VADM1 hydrogel, its ability to block ruptured arteries must be considered. The abdominal aorta of rats was first peeled from the surrounding tissues and closed end-to-end with artery clamps (Fig. 5c1). It was then clipped using surgical scissors, revealing large regions of hemorrhage after the clip was released (Fig. 5c2-c3). Then clipped the ruptured artery, 2 mL of VADM1 was injected into the bleeding site (Fig. 5c4), and the ruptured artery was surrounded by the VADM1 hydrogel (Fig. 5c5). The artery clamp was removed after 5 min, and the hemorrhage stopped (Fig. 5c6). Interestingly, when the VADM1 hydrogels were removed, the broken end of the abdominal aorta continued to pulsate but did not bleed. This is because the hydrogel seals the ruptured blood vessels. Fig. 5c7–c9 shows the mass of blood spouting from the ruptured vessel without the intervention of the hydrogel. These results demonstrate the potential of the hydrogel in stopping the hemorrhaging of ruptured vessels, even in regions like the abdominal aorta with the strongest blood-flow velocity. It covers not only injury following the trauma but also occult vascular injury during surgery.

To explore the hemostasis mechanism of the hydrogels, the incision of liver, the tissue-defect of kidney and the broken end of the abdominal aorta treated with VADM1 were washed and stained using the HE method. The staining results showed significant cell accumulation in the trauma (Fig. 5d). In our work, the hemostasis process of VADM hydrogel contained two steps. First, when the hydrogel encounters the wound, it changes from liquid to solid to form a physical barrier to prevent further blood flow. Its potential mechanism may be as described by Nyambat Batzaya [51]. Both the storage modulus (G') and the loss modulus (G'') increase with the temperature rise from $10°C$ to $37°C$ in hydrogels, promoting the transformation from liquid phase to solid phase. Subsequently, extra-cellular matrix components (include collagen, fibronectin, laminin and other ECM proteins) are important mediators for thrombosis [30] to promote blood coagulation together. So ECM hydrogel is an effective hemostatic material.

3.7. Staphylococcus aureus-infected skin wound healing by antibacterial hydrogel

Extracellular matrix hydrogels are rich in collagen, glycosaminoglycan, bone morphogenetic protein, growth factors, etc., which promote the repair of skin tissue defects [29]. Therefore, after being loaded with vancomycin, VADM hydrogel can not only promote skin tissue healing, but also play an anti-infection effect. A skin-wound model with *S. aureus* infection was established on the backs of the rat subjects. The wound was then sealed with each VADM hydrogel separately. The untreated incision and the ADM hydrogel were used as the control groups. Fig. 6a illustrates the healing process. On day 7, the edges of all the groups started to contract. The wounds treated with VADM1, VADM2, VADM4, and VADM6 became significantly smaller than those in the control group. On day 14, all the wounds in the six groups were closed, and VADM1, VADM2, VADM4, and VADM6 had the best healing performance compared with the control groups.

Wound closure rates based on the wound area were quantitatively calculated, as shown in Fig. 6c. On day 7, compared with the wound closure rates in the untreated and ADM-treated groups ($51.37 \pm 5.04\%$ and $58.45 \pm 8.30\%$, respectively), the wound closure rates in the VADM1, VADM2, VADM4, and VADM6 groups significantly increased to $87.29 \pm 1.84\%$, $87.65 \pm 3.45\%$, $86.97 \pm 6.90\%$, and $87.56 \pm 4.27\%$, respectively ($p < 0.05$). On day 14, the untreated and ADM-treated wounds displayed closure rates of $72.25 \pm 1.92\%$ and $85.13 \pm 3.21\%$, respectively. VADM1, VADM2, VADM4, and VADM6 had higher closure rates of $97.96 \pm 0.63\%$, $96.76 \pm 1.06\%$, $96.6 \pm 0.67\%$, and $96.34 \pm 0.63\%$, respectively. The healing tissue was stained with H&E to

further investigate the histopathological structure during wound healing between these groups. On day 7, numerous inflammatory cells appeared in the untreated wound and ADM groups, more than those in the VADM1, VADM2, VADM4, and VADM6 groups (Fig. 6b). Immunohistochemical staining for CD68^{+} macrophages and myeloperoxidase (MPO)-labeled neutrophils reveals the infiltration of neutrophils and macrophages into the trauma (Fig. 6d). On day 14, the untreated and ADM groups contained many inflammatory cells and a few myofibroblasts, whereas the vancomycin-loaded ADM groups had few inflammatory cells and lots of myofibroblasts. The hair follicle-like histopathological structures can be seen in the VADM1 and VADM2 groups.

4. Conclusion

We designed a porcine ADM hydrogel loaded with vancomycin as an antimicrobial agent. The hydrogel's physical adsorption property allows for the local rapid release of vancomycin. The cumulative release rate is approximately 80% within 1 h. This demonstrates a strong antibacterial effect in the early stage of trauma healing. *In vivo* hemostasis experiments on rats demonstrated the hydrogel's ability to effectively control hemorrhage and prevent blood vessel damage. Thus, vancomycin-loaded porcine ADM hydrogel has been demonstrated as a potential biomaterial for hemorrhage control and bacterial infection prevention in trauma and occult vascular injuries.

Credit author statement

Bin Fang, Lei Lu and Dan Zu guided all the experiments. Dan Cai, Sunfang Chen and Bing Wu prepared acellular porcine skin hydrogel and completed the characterization analysis. Jianjiang Chen was responsible for bacteriological examination, Danhua Tao and Zhiqing Li completed the pathological examination of the tissues, and the animal experiments were completed by Qidong and Yubin Zou. Yating Chen and Chenchen Bi performed all the cytology related experiments.

Declaration of competing interest

The authors declare that they have no known competing financial interests or personal relationships that could have appeared to influence the work reported in this paper

Acknowledgments

References

[1] D. Kauvar, R. Lefering, C. Wade, Impact of hemorrhage on trauma outcome: an overview of epidemiology, clinical presentations, and therapeutic considerations, J. Trauma 60 (2006) S3–S11, https://doi.org/10.1097/01.ta.0000199961.02677.19.

[2] G. Patil, A. Torris, P. Suresha, S. Jadhav, M. Badiger, V. Ghormade, Design and synthesis of a new topical agent for halting blood loss rapidly: a multimodal chitosan–gelatin xerogel composite loaded with silica nanoparticles and calcium, Colloids Surf. B Biointerfaces 198 (2021) 111454, https://doi.org/10.1016/j.colsurfb.2020.111454.

[3] B. Haas, A.B. Nathens, Pro/con debate: is the scoop and run approach the best approach to trauma services organization? Crit. Care (London, England) 12 (2008) 224, https://doi.org/10.1186/cc6980.

[4] Y. Wang, Y. Zhao, L. Qiao, F. Zou, Y. Xie, Y. Zheng, Y. Chao, Y. Yang, W. He, S. Yang, Cellulose fibers-reinforced self-expanding porous composite with multiple hemostatic efficacy and shape adaptability for uncontrollable massive hemorrhage treatment, Bioact. Mater. 6 (2021) 2089–2104, https://doi.org/10.1016/j.bioactmat.2020.12.014.

[5] J. Li, W. Cao, X. Lv, L. Jiang, Y. Li, W. Li, S. Chen, X. Li, Zeolite-based hemostat QuikClot releases calcium into blood and promotes blood coagulation in vitro, Acta Pharmacol. Sin. 34 (2013) 367–372, https://doi.org/10.1038/aps.2012.159.

[6] B. Kozen, S. Kircher, J. Henao, F. Godinez, A. Johnson, An alternative hemostatic dressing: comparison of CELOX, HemCon, and QuikClot, Acad. Emerg. Med. 15 (2008) 74–81, https://doi.org/10.1111/j.1553-2712.2007.00009.x.

[7] B. Hsu, S. Hagerman, K. Jamieson, S. Castleberry, W. Wang, E. Holler, J. Ljubimova, P. Hammond, Multifunctional self-assembled films for rapid hemostat and sustained anti-infective delivery, ACS Biomater. Sci. Eng. 1 (2015) 148–156, https://doi.org/10.1021/ab500050m.

[8] C.K. Murray, Infectious disease complications of combat-related injuries, Crit. Care Med. 36 (2008) S358–S364, https://doi.org/10.1097/CCM.0b013e31817e2ffc.

[9] Y. Bu, L. Zhang, J. Liu, L. Zhang, T. Li, H. Shen, X. Wang, F. Yang, P. Tang, D. Wu, Synthesis and properties of hemostatic and bacteria-responsive in situ hydrogels for emergency treatment in critical situations, ACS Appl. Mater. Interfaces 8 (2016) 12674–12683, https://doi.org/10.1021/acsami.6b03235.

[10] S. Ryu, P. Song, C. Seo, H. Cheong, Y. Park, Colonisation and infection of the skin by S. aureus: immune system evasion and the response to cationic antimicrobial peptides, Int. J. Mol. Sci. 15 (2014) 8753–8772, https://doi.org/10.3390/ijms15058753.

[11] S. Casu, D. Häske, Severe sepsis and septic shock in pre-hospital emergency medicine: survey results of medical directors of emergency medical services concerning antibiotics, blood cultures and algorithms, Intern. Emerg. Med. 11 (2016) 571–576, https://doi.org/10.1007/s11739-015-1371-9.

[12] M. Fan, J. Si, X. Xu, L. Chen, J. Chen, C. Yang, J. Zhu, L. Wu, J. Tian, X. Chen, X. Mou, X. Cai, A versatile chitosan nanogel capable of generating AgNPs in-situ and long-acting slow-release of Ag+ for highly efficient antibacterial, Carbohydr. Polym. 257 (2021) 117636, https://doi.org/10.1016/j.carbpol.2021.117636.

[13] I. Ketikidis, C.N. Banti, N. Kourkoumelis, C.G. Tsiafoulis, C. Papachristodoulou, A.G. Kalampounias, S.K. Hadjikakou, Conjugation of penicillin-G with silver(I) ions expands its antimicrobial activity against gram negative bacteria, Antibiotics (Basel, Switzerland) 9 (2020) 25, https://doi.org/10.3390/antibiotics9010025.

[14] Y. Zhang, Y. Chen, L. Huang, Z. Chai, L. Shen, Y. Xiao, The antifungal effects and mechanical properties of silver bromide/cationic polymer nano-composite-modified Poly-methyl methacrylate-based dental resin, Sci. Rep. 7 (2017) 1547, https://doi.org/10.1038/s41598-017-01686-4.

[15] S. Ong, J. Wu, S. Moochhala, M. Tan, J. Lu, Development of a chitosan-based wound dressing with improved hemostatic and antimicrobial properties, Biomaterials 29 (2008) 4323–4332, https://doi.org/10.1016/j.biomaterials.2008.07.034.

[16] X.F. Zhang, W. Shen, S. Gurunathan, Silver nanoparticle-mediated cellular responses in various cell lines: an in vitro model, Int. J. Mol. Sci. 17 (2016) 1603, https://doi.org/10.3390/ijms17101603.

[17] Y. Cho, Y. Mizuta, J. Akagi, T. Toyoda, M. Sone, K. Ogawa, J. Toxicol. Pathol. 31 (2018) 73–80, https://doi.org/10.1293/tox.2017-0043.

[18] L. Hazeem, G. Kuku, E. Dewailly, C. Slomianny, A. Barras, A. Hamdi, R. Boukherroub, M. Culha, M. Bououdina, Toxicity effect of silver nanoparticles on photosynthetic pigment content, growth, ROS production and ultrastructural changes of microalgae chlorella vulgaris, Nanomaterials 9 (2019) 914, https://doi.org/10.3390/nano9070914.

[19] T. Park, S. Lee, R. Amatya, H. Cheong, C. Moon, H. Kwak, K. Min, M. Shin, ICG-loaded PEGylated BSA–silver nanoparticles for effective photothermal cancer therapy, Int. J. Nanomed. 15 (2020) 5459–5471, https://doi.org/10.2147/IJN.S255874.

[20] F. Monedeiro, P. Pomastowski, M. Milanowski, T. Ligor, B. Buszewski, Monitoring of bactericidal effects of silver nanoparticles based on protein signatures and VOC emissions from Escherichia coli and selected salivary bacteria, J. Clin. Med. 8 (2019) 2024, https://doi.org/10.3390/jcm8112024.

[21] S. Kim, J. Choi, J. Choi, K. Chung, K. Park, J. Yi, D. Ryu, Oxidative stress-dependent toxicity of silver nanoparticles in human hepatoma cells, Toxicol. Vitro 23 (2009) 1076–1084, https://doi.org/10.1016/j.tiv.2009.06.001.

[22] T. Zhang, L. Wang, Q. Chen, C. Chen, Cytotoxic potential of silver nanoparticles, Yonsei Med. J. 55 (2014) 283–291, https://doi.org/10.3349/ymj.2014.55.2.283.

[23] P. Skallerup, C. Espinosa-Gongora, C. Jørgensen, L. Guardabassi, M. Fredholm, Genome-wide association study reveals a locus for nasal carriage of Staphylococcus aureus in Danish crossbred pigs, BMC Vet. Res. 11 (2015) 290, https://doi.org/10.1186/s12917-015-0599-y.

[24] E. Esfahanian, U. Adhikari, K. Dolan, J. Mitchell, Construction of a new dose–response model for Staphylococcus aureus considering growth and decay kinetics on skin, Pathogens 8 (2019) 253, https://doi.org/10.3390/pathogens8040253.

[25] K. Thitiananpakorn, Y. Aiba, X. Tan, S. Watanabe, K. Kiga, Y. Sato'o, T. Boonsiri, F. Li, T. Sasahara, Y. Taki, A. Azam, Y. Zhang, L. Cui, Association of mprF mutations with cross-resistance to daptomycin and vancomycin in methicillin-resistant Staphylococcus aureus (MRSA), Sci. Rep. 10 (2020) 16107, https://doi.org/10.1038/s41598-020-73108-x.

[26] J. Won, M. Lee, M. Kim, K. Min, G. Ahn, J. Han, S. Jin, W. Yun, J. Shim, A potential dermal substitute using decellularized dermis extracellular matrix derived bio-ink, Artif. Cells Nanomed. Biotechnol. 47 (2019) 644–649, https://doi.org/10.1080/21691401.2019.1575842.

[27] R. Chen, H. Ho, Y. Tsai, M. Sheu, Process development of an acellular dermal matrix (ADM) for biomedical applications, Biomaterials 25 (2004) 2679–2686, https://doi.org/10.1016/j.biomaterials.2003.09.070.

[28] K. Bankoti, A. Rameshbabu, S. Datta, M. Roy, P. Goswami, S. Roy, A. Das, S. Ghosh, S. Dhara, Carbon nanodot decorated acellular dermal matrix hydrogel augments chronic wound closure, J. Mater. Chem. B 8 (2020) 9277–9294, https://doi.org/10.1039/D0TB01574A.

[29] M. Spang, K. Christman, Extracellular matrix hydrogel therapies: in vivo applications and development, Acta Biomater. 68 (2018) 1–14, https://doi.org/10.1016/j.actbio.2017.12.019.

[30] H. Wang, Y. Ye, W. Wan, L. Wang, R. Li, L. Li, L. Yang, L. Yang, Y. Gu, L. Dong, Z. Meng, Xinmailong modulates platelet function and inhibits thrombus formation via the platelet αiibβ3-mediated signaling pathway, Front. Pharmacol. 10 (2019) 923, https://doi.org/10.3389/fphar.2019.00923.

[31] R. Albright, W. Chang, D. Robert, D. Ornstein, W. Cao, L. Liu, M. Redick, J. Young, E. de la Cruz, D. Braddock, NPP4 is a procoagulant enzyme on the surface of vascular endothelium, Blood 120 (2012) 4432–4440, https://doi.org/10.1182/blood-2012-04-425215.

[32] J. Jang, S. Wang, J. Min, Y. Chae, J. Baek, D. Yu, T. Chang, Peroxiredoxin II is an antioxidant enzyme that negatively regulates collagen-stimulated platelet function, J. Biol. Chem. 290 (2015) 11432–11442, https://doi.org/10.1074/jbc.M115.644260.

[33] Y. Wang, R. Gallant, H. Ni, Extracellular matrix proteins in the regulation of thrombus formation, Curr. Opin. Microbiol. 23 (2016) 280–287, https://doi.org/10.1097/MOH.0000000000000237.

[34] J. Hu, I. Altun, Z. Zhang, H. Albadawi, M. Salomao, J. Mayer, L. Hemachandra, S. Rehman, R. Oklu, Bioactive-tissue-derived nanocomposite hydrogel for permanent arterial embolisation and enhanced vascular healing, Adv. Mater. 32 (2020), e2002611, https://doi.org/10.1002/adma.202002611.

[35] S. Guan, Y. Li, C. Cheng, X. Gao, X. Gu, X. Han, H. Ye, Manufacture of pH- and HAase-responsive hydrogels with on-demand and continuous antibacterial activity for full-thickness wound healing, Int. J. Biol. Macromol. 164 (2020) 2418–2431, https://doi.org/10.1016/j.ijbiomac.2020.08.108.

[36] Y. Wang, C. Dou, G. He, L. Ban, L. Huang, Z. Li, J. Gong, J. Zhang, P. Yu, Biomedical Potential of ultrafine Ag nanoparticles coated on poly (gamma-glutamic acid) hydrogel with special reference to wound healing, Nanomaterials 8 (2018) 324, https://doi.org/10.3390/nano8050324.

[37] J. Hoque, B. Bhattacharjee, R. Prakash, K. Paramanandham, J. Haldar, Dual function injectable hydrogel for controlled release of antibiotic and local antibacterial therapy, Biomacromolecules 19 (2018) 267–278, https://doi.org/10.1021/acs.biomac.7b00979.

[38] Y. Li, G. Li, X. Sha, L. Li, K. Zhang, D. Liu, Y. Hao, X. Cui, L. Wang, H. Wang, An intelligent vancomycin release system for preventing surgical site infections of bone tissues, Biomater. Sci. 8 (2020) 3202–3211, https://doi.org/10.1039/D0BM00255K.

[39] A. Ghimire, J. Skelly, J. Song, Micrococcal-nuclease-triggered on-demand release of vancomycin from intramedullary implant coating eradicates Staphylococcus aureus infection in mouse femoral canals, ACS Cent. Sci. 5 (2019) 1929–1936, https://doi.org/10.1021/acscentsci.9b00870.

[40] B. Fang, P. Qiu, C. Xia, D. Cai, C. Zhao, Y. Chen, H. Wang, S. Liu, H. Cheng, Z. Tang, B. Wang, S. Fan, X. Lin, Extracellular matrix scaffold crosslinked with vancomycin for multifunctional antibacterial bone infection therapy, Biomaterials 268 (2021) 120603, https://doi.org/10.1016/j.biomaterials.2020.120603.

[41] C. Ketonis, S. Barr, I. Shapiro, J. Parvizi, C. Adams, N. Hickok, Antibacterial activity of bone allografts: comparison of a new vancomycin-tethered allograft with allograft loaded with adsorbed vancomycin, Bone 48 (2011) 631–638, https://doi.org/10.1016/j.bone.2010.10.171.

[42] P. Colavite-Machado, L. Ishikawa, T. França, S. Zorzella-Pezavento, L. da Rosa, F. Chiuso-Minicucci, M.L. da Cunha, G. Garlet, A. Sartori, Differential arthritogenicity of Staphylococcus aureus strains isolated from biological samples, BMC Infect. Dis. 13 (2013) 400, https://doi.org/10.1186/1471-2334-13-400.

[43] A. Cheng, M. McAdow, H. Kim, T. Bae, D. Missiakas, O. Schneewind, Contribution of coagulases towards Staphylococcus aureus disease and protective immunity, PLoS Pathog. 6 (2010), e1001036, https://doi.org/10.1371/journal.ppat.1001036.

[44] A. Kengmo Tchoupa, A. Peschel, Staphylococcus aureus releases proinflammatory membrane vesicles to resist antimicrobial fatty acids, mSphere 5 (2020), https://doi.org/10.1128/mSphere.00804-20.

[45] S. Jorch, B. Surewaard, M. Hossain, M. Peiseler, C. Deppermann, J. Deng, A. Bogoslowski, F. van der Wal, A. Omri, M. Hickey, P. Kubes, Peritoneal GATA6+ macrophages function as a portal for Staphylococcus aureus dissemination, J. Clin. Invest. 129 (2019) 4643–4656, https://doi.org/10.1172/JCI127286.

[46] W. Liu, W. Ou-Yang, C. Zhang, Q. Wang, X. Pan, P. Huang, C. Zhang, Y. Li, D. Kong, W. Wang, Synthetic polymeric antibacterial hydrogel for methicillin-resistant staphylococcus aureus-infected wound healing: nanoantimicrobial self-assembly, drug- and cytokine-free strategy, ACS Nano 14 (2020) 12905–12917, https://doi.org/10.1021/acsnano.0c03855.

[47] X. Fan, Y. Li, N. Li, G. Wan, M. Ali, K. Tang, Rapid hemostatic chitosan/cellulose composite sponge by alkali/urea method for massive haemorrhage, Int. J. Biol. Macromol. 164 (2020) 2769–2778, https://doi.org/10.1016/j.ijbiomac.2020.07.312.

[48] K. Tsuji, K. Kimura, K. Tateda, H. Takahashi, Does vitamin D3 prevent the inhibitory effect of vancomycin on osteoblasts? Clin. Orthop. Relat. Res. 478 (2020) 420–433, https://doi.org/10.1097/CORR.0000000000001060.

[49] Y. Zhang, L. Shen, Z. Mao, N. Wang, X. Wang, X. Huang, Y. Hu, D. Shou, C. Wen, Icariin enhances bone repair in rabbits with bone infection during post-infection treatment and prevents inhibition of osteoblasts by vancomycin, Front. Pharmacol. 8 (2017) 784, https://doi.org/10.3389/fphar.2017.00784.

[50] J. Qiu, X. Niu, J. Wang, Y. Xing, B. Leng, J. Dong, H. Li, M. Luo, Y. Zhang, X. Dai, Y. Luo, X. Deng, Capsaicin protects mice from community-associated methicillin-resistant Staphylococcus aureus pneumonia, PLoS One 7 (2012), e33032, https://doi.org/10.1371/journal.pone.0033032.

[51] B. Nyambat, Y.B. Manga, C.H. Chen, U. Gankhuyag, Wp A Pratomo, M. Kumar Satapathy, E.Y. Chuang, New insight into natural extracellular matrix: genipin cross-linked adipose-derived stem cell extracellular matrix gel for tissue engineering, Int. J. Mol. Sci. 21 (2020) 4864, https://doi.org/10.3390/ijms21144864.

[52] L.T. Saldin, M.C. Cramer, S.S. Velankar, L.J. White, S.F. Badylak, Extracellular matrix hydrogels from decellularized tissues: structure and function, Acta Biomater. 49 (2017) 1–15, https://doi.org/10.1016/j.actbio.2016.11.068.

[53] P. Collignon, P.C. Athukorala, S. Senanayake, F. Khan, Antimicrobial resistance: the major contribution of poor governance and corruption to this growing problem, PloS One 10 (2015), e0116746, https://doi.org/10.1371/journal.pone.0116746.

[54] X.N. Zhang, Z.J. Ma, Y. Wang, B. Sun, X. Guo, C.Q. Pan, L.M. Chen, Angelica Dahurica ethanolic extract improves impaired wound healing by activating angiogenesis in diabetes, PloS One 12 (2017), e0177862, https://doi.org/10.1371/journal.pone.0177862.

[55] Byoung Soo Kim, Sanskrita Das, Jinah Jang, Cho Dong-Woo, Decellularized extracellular matrix-based bioinks for engineering tissue- and organ-specific microenvironments, Chem. Rev. 120 (2020) 10608–10661. https://doi:10.1021/acs.chemrev.9b00808.

[56] Coen Maas, José W.P. Govers-Riemslag, Barend Bouma, Bettina Schiks, P.C. Hazenberg Bouke, Henk M. Lokhorst, Per Hammarström, Hugo ten Cate, Philip G. de Groot, Bonno N. Bouma, F.B.G. Gebbink Martijn, Misfolded proteins activate factor XII in humans, leading to kallikrein formation without initiating coagulation, J. Clin. Invest. 118 (2008) 3208–3218. http://doi:10.1172/JCI35424.

[57] Karl E. Kadler, Adele Hill, Elizabeth G. Canty-Laird, Collagen fibrillogenesis: fibronectin, integrins, and minor collagens as organizers and nucleators, Curr. Opin. Cell Biol. 20 (2008) 495–501, https://doi.org/10.1016/j.ceb.2008.06.008.

[58] D. Honová, Spectrophotometric determination of bismuth and EDTA by means of the reaction of bismuth with pyrocatechol violet in the presence of septonex, Talanta 35 (1988) 803–804. http://doi:10.1016/0039-9140(88)80187-5.

[59] Maroya Spalding Walters, Paula Eggers, Valerie Albrecht, Tatiana Travis, David Lonsway, Greg Hovan, Debra Taylor, Kamile Rasheed, Brandi Limbago, Alexander Kallen, Vancomycin-Resistant Staphylococcus aureus - Delaware, 2015, MMWR Morb. Mortal. Wkly. Rep. 64 (2015) 1056. https://doi.org/10.15585/mmwr.mm6437a6.